

1 **The impact of human-induced climate change on future tornado intensity as revealed**
2 **through multi-scale modeling**

3

4 **Matthew J. Woods^{1†}, Robert J. Trapp², and Holly M. Mallinson³**

5 ¹Department of Atmospheric Sciences, University of Illinois.

6 ²Department of Atmospheric Sciences, University of Illinois.

7 ³Department of Atmospheric Sciences, University of Illinois.

8

9 Corresponding author: Robert J. Trapp (jtrapp@illinois.edu)

10 †Current affiliation: National Weather Service, Las Vegas, NV.

11

12

13 **Key Points:**

- 14
- The effects of climate change on tornado intensity have been unclear.
 - A novel, multi-modeling approach is used to address such effects.
 - The intensity of cool-season tornadoes would appear to be most susceptible.
- 15
16
17

18 **Abstract**

19 A novel, multi-scale climate modeling approach is used to show the potential for increases in
20 future tornado intensity due to anthropogenic climate change. Historical warm- and cool-season
21 (WARM and COOL) tornado events are virtually placed in a globally warmed future via the
22 “pseudo-global warming” method. As hypothesized based on meteorological arguments, the
23 tornadic-storm and associated vortex of the COOL event experiences consistent and robust
24 increases in intensity, and size in an ensemble of imposed climate-change experiments. The
25 tornadic-storm and associated vortex of the WARM event experiences increases in intensity in
26 some of the experiments, but the response is neither consistent nor robust, and is overall weaker
27 than in the COOL event. An examination of environmental parameters provides further support
28 of the disproportionately stronger response in the cool-season event. These results have
29 implications on future tornadoes forming outside of climatologically favored seasons.

30

31 **1 Introduction**

32 Hazardous convective weather (HCW) in the form of damaging winds, hail, and tornadoes
33 poses a serious threat to life and property in the United States. From 2012 to 2022, 99 HCW events
34 each produced over \$1 billion (inflation-adjusted) in damages (NOAA, 2022). The frequency of
35 these billion-dollar events has increased markedly since the start of the 21st century, owing in part
36 to increased exposure and population density (Strader et al., 2017), but also potentially to
37 anthropogenic climate change (ACC).

38 HCW depends on the 3D characteristics of environmental temperature, humidity, and
39 wind, which appear to have changed over the last few decades (Gensini & Brooks, 2018; Tang et
40 al. 2019; Taszarek et al., 2021) and are projected to change further by the late 21st century under
41 ACC. For example, as shown by Trapp et al. (2007), warming and humidification of lower-
42 tropospheric air yields increases in convective available potential energy (CAPE), which leads to
43 increases in the potential intensity of convective-storm updrafts. Conversely, relatively more
44 warming at high latitudes weakens the meridional temperature gradient and thus weakens the
45 vertical shear of the horizontal wind (hereinafter, VWS) per the thermal wind relation (e.g., Trapp
46 et al. 2007); this suggests a reduction in the tendency for convective updrafts to develop significant,

47 long-lived rotational cores. General circulation model (GCM) and regional climate model (RCM)
48 simulations reveal decreases in VWS that are disproportionately smaller than increases in CAPE,
49 indicating an increase in frequency and/or intensity of future HCW events under ACC in the United
50 States (e.g., Trapp et al., 2007; Del Genio et al., 2007; Trapp et al., 2009; Diffenbaugh et al., 2013;
51 Gensini et al., 2014; Seeley & Romps, 2015; Hoogewind et al., 2017). Of relevance herein is the
52 seasonal non-uniformity to this increase: Boreal winter tends to exhibit the largest relative increase
53 in the CAPE–VWS covariate (Diffenbaugh et al., 2013). This is consistent with historical trends
54 of environmental parameters computed using reanalysis data (Gensini & Brooks, 2018).

55 Precisely how these conclusions relate to *tornado intensity*, and thus address the very basic
56 question of whether the environmental conditions due to 21st century ACC will contribute to more
57 intense tornadoes, is unclear. This is partly because relationships between observed tornado
58 intensity and environmental parameters such as CAPE and VWS are ambiguous. For example,
59 although nonzero CAPE is considered a necessary condition for, and thus critically relevant to
60 tornadic-storm formation, CAPE alone does not correlate well with observed tornado intensity
61 (Thompson et al., 2012). As supported by our analyses in section 3.3, a possible link could be
62 made using multivariate environmental parameters such as the significant tornado parameter
63 (STP), which appears to better discriminate environments of significant tornadoes from those of
64 nonsignificant tornadoes (Thompson et al., 2012), although still not perfectly. However, an
65 environment-only argument has a critical limitation, namely, that realization of a significant
66 tornado is conditional on tornadic-storm initiation, which STP does not unambiguously predict.
67 Indeed, the mean frequency of storms that initiate given a supportive environment is non-uniform
68 in time and space, and even appears to change under late 21st century ACC (Hoogewind et al.,
69 2017).

70 Explicit climate modeling of tornadoes is an alternative to the use of environmental
71 parameters and removes the storm-initiation limitation. Although such an approach has been
72 computationally prohibitive because of the small-scale of tornadoes (~100 m to 1 km), multi-scale
73 modeling now offers a tractable solution. Herein we follow Trapp & Hoogewind (2016) and
74 employ the pseudo global warming (PGW) method (Schär et al., 1996; Frei et al., 1998; Kimura
75 and Kitoh, 2007; Sato et al., 2007) using a novel, multi-scale, multi-model approach. Briefly, the
76 PGW method involves a comparison of simulations of events under their true 4D environment (the
77 control; CTRL) with those under a 4D environment modified by a climate-change perturbation
78 representative of *mean atmospheric conditions* over future (here, late 21st century) and historical
79 (here, late 20th century) time slices. Thus, this method allows for an isolation of the response of
80 an event to an imposed environment of the future. Because *event-level* PGW applications (see
81 Trapp et al., 2021) involve relatively short time integrations, they also allow for the use of higher
82 resolution and multiple realizations.

83 Two archetypal yet regionally and seasonally contrasting events are considered. The first
84 is the 10 February 2013 (hereinafter, COOL) event that includes the EF-4 tornado in Hattiesburg,
85 Mississippi, and the second is the 20 May 2013 (hereinafter, WARM) event that includes the EF-
86 5 tornado in Moore, Oklahoma. Together, these tornadoes were responsible for 24 fatalities, more
87 than 300 injuries, and approximately \$2 billion in damage (NOAA, 2013). Our working hypothesis
88 is that the WARM event will exhibit relatively less intensity changes under PGW than the COOL
89 event.

90 Analyses of these event simulations provide the initial means to address this hypothesis.
91 However, the spatio-temporal representations of the tornadic storms, and even the total numbers
92 of storms, are different between the PGW and CTRL simulations (see Fig. 1). This implied lack

93 of a clear CTRL-to-PGW comparison of *specific* tornadic storms means that a quantitative
94 evaluation of the climate change effect on the intensity of *specific* tornadoes is tenuous.
95 Accordingly, we introduce an additional step wherein an idealized numerical model is integrated
96 using initial and boundary conditions (ic/bc) drawn from the regional-model simulations. The
97 relatively reduced complexity and higher spatial resolutions afforded by this idealized-modeling
98 implementation of the PGW methodology helps further isolate the climate change response on a
99 single storm, and allows for explicit diagnoses of tornado intensity.

100 **2 Materials and Methods**

101 2.1 PGW

102 The PGW method involves simulations of some event wherein its actual, present-day
103 forcing is modified through the addition of a climate-change perturbation or “delta”, which is the
104 difference between mean conditions over future and historical time slices during a relevant month.
105 Separate sets of deltas are constructed using historical and Representative Concentration Pathway
106 8.5 simulations from each of five GCMs (GFDL-CM3, MIROC5, NCAR-CCSM4, IPSL-CM5A-
107 LR, and NorESM-1M). The GCM data originate from the Coupled Model Intercomparison Project
108 phase 5 (Taylor et al., 2012), and provide a range of convective-storm environments over historical
109 and future time periods (e.g., see Diffenbaugh et al., 2013; Seeley & Romps, 2015).

110 Three different formulations of the climate-change deltas (see Trapp et al., 2021),
111 computed using five different GCMs, provide an ensemble of 15 simulations plus an additional
112 composite-delta simulation to assess the PGW response of each event. Because these 16 different
113 deltas explicitly represent a range in the climate-change signal, we argue that their use toward
114 generation of an ensemble is more relevant than other approaches. Specifically, and importantly,

115 we are interested in the model response to the imposed future climate change and associated ic/bc
116 rather than in the model response to variations in parameterization schemes, etc.

117

118 2.2 Regional model configuration

119 The CTRL and PGW simulations of the WARM and COOL events are performed using
120 version 4.0 of the Weather Research and Forecasting model (WRF) (Skamarock et al., 2008).

121 The parent computational domains have horizontal grid spacings of 3 km. Subdomains of 1-km
122 grid spacing are nested within the parent domains over central Oklahoma and central Mississippi,
123 respectively (Fig. S1). The results reported in section 3.1 are based on analyses over the nested
124 domains.

125 The simulations are initialized at 12 UTC for both events. This allows for more than six
126 hours of “spin-up” time prior to the observed EF-5 Moore (~2000 UTC) and EF-4 Hattiesburg
127 (~2300 UTC) tornadoes, which is typical for weather-event simulations with WRF (Skamarock,
128 2004). Initial and boundary conditions are derived from the North American Mesoscale Forecast
129 System analysis. Additional details regarding the WRF configuration can be found in Trapp et al.
130 (2021). Decisions on the configuration and on the ultimate veracity of the CTRL simulations
131 were established by comparing model output from configuration-sensitivity experiments to
132 observed radar characteristics and tornado reports, as described in Woods (2021).

133 Tornadoes are not resolved on model grids with 1-km spacings. However, as
134 demonstrated in the Supplement, their signatures and potential intensity can be inferred using
135 vertical vorticity (VV) computed at 80 m AGL, which is approximately the height of the first
136 level above the lower boundary of the model. A VV value locally exceeding $7.5 \times 10^{-3} \text{ s}^{-1}$, which
137 is the 99th percentile of gridpoint values in the CTRL simulation, serves as a tornado proxy

138 occurrence. A VV value exceeding $1.25 \times 10^{-2} \text{ s}^{-1}$, which is the 99.9th percentile, serves as a
139 significant tornado proxy occurrence. Coexistence of local updraft velocities exceeding 5 m s^{-1} is
140 also required, to ensure that the VV is associated with a convective updraft. Differentiating
141 tornado intensity based on VV is justified in the Supplement through an analyses of a vortex
142 model, and also follows from Doppler radar-based studies by Toth et al. (2012) and others.

143

144 2.3 Idealized model configuration

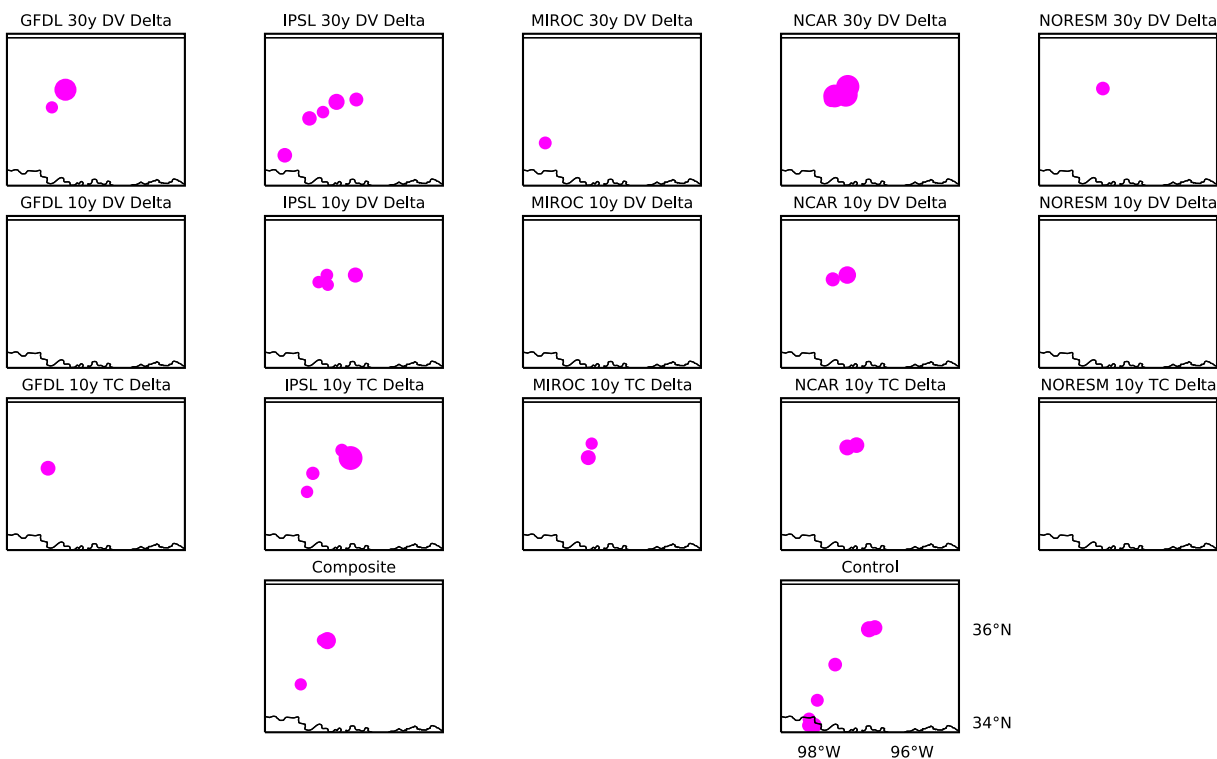
145 The idealized simulations are performed using Cloud Model 1 (CM1) (Bryan & Fritsch,
146 2002). Grid stretching is employed such that the horizontal grid spacing is 64 m over the inner 80
147 x 80 km of the 180 x 180 x 18.5 km model domain, and then increased to 2.5 km at the domain
148 edges. Vertical grid spacing varies from 20 m in the lowest model levels to 250 m in the upper
149 levels. Additional details regarding the CM1 model configuration can be found in Woods
150 (2021). Note that the actual tornadoes that occurred on 20 May 2013 and 10 February 2013 had
151 damage widths of 1600 m and 1200 m, respectively. Even if the core diameters of maximum
152 winds of these tornadoes were 50% of these widths, the cores would still be represented by ~ 10
153 grid points. So, although our simulations do not have grid spacings appropriate to resolve fine-
154 scale structures of the tornadoes, the simulations are certainly sufficient to represent core widths
155 and windspeeds, which is one goal of these simulations.

156 The initial and boundary conditions are drawn from the WRF output of the CTRL and
157 PGW simulations. Specifically, 60 x 60 km horizontal averages centered about the WRF grid
158 point nearest to Moore, Oklahoma and Hattiesburg, Mississippi are used to obtain vertical
159 profiles at 20 UTC 20 May 2013 and 23 UTC 10 February, respectively, which represent the pre-
160 tornadic conditions during these two events. A single deep convective storm is initiated within

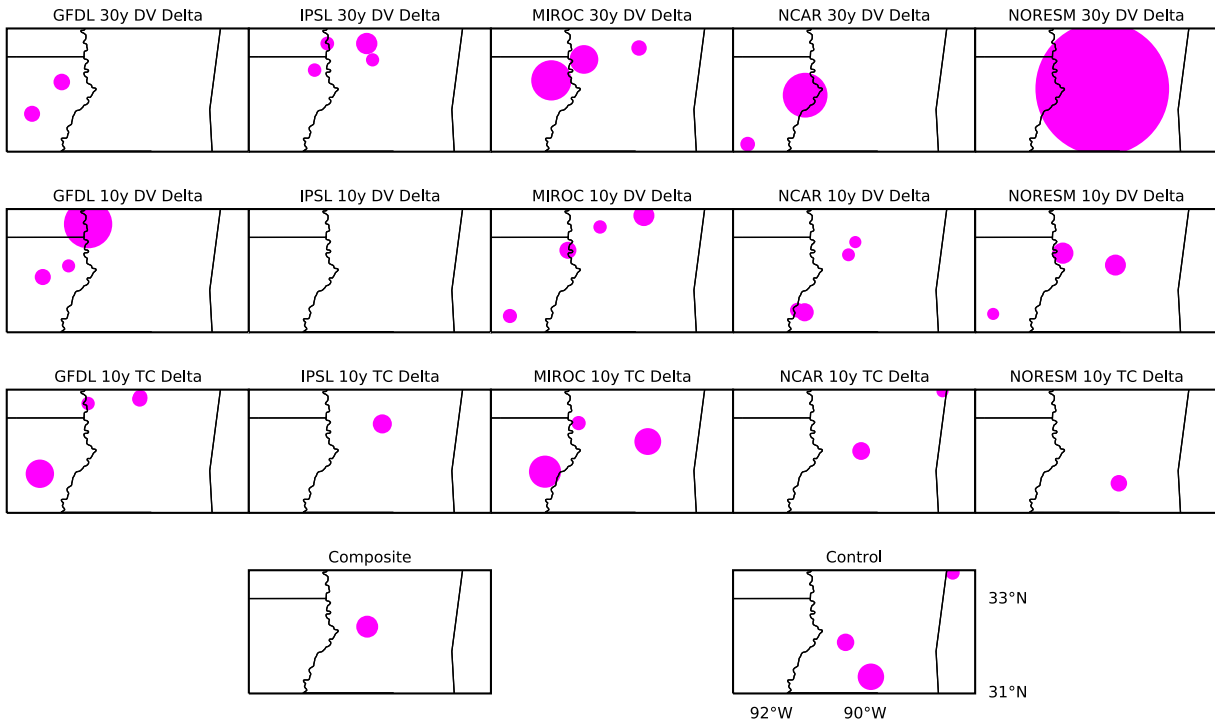
161 these environments via updraft nudging (Naylor & Gilmore, 2012) that persisted for 20 minutes.
 162 Our analysis of the subsequent tornadic circulations begins at 30 min, i.e., 10 min after the
 163 cessation of the nudging.

164 Tornadic-like vortices (TLVs) are identified by examining near-surface fields of
 165 windspeed, VV , and the Obuko-Weiss (OW) parameter. Adapting the approaches of Sherburn &
 166 Parker (2019), Gray & Frame (2021), and others, TLV identification requires VV , windspeed,
 167 and OW to exceed 0.1 s^{-1} , 30 m s^{-1} , and 0.03 s^{-2} , respectively, and be collocated with low-level
 168 updraft speeds exceeding 5 m s^{-1} . Upon locating the strongest TLV, maximum and minimum of
 169 x -direction and y -direction wind components are found within 500 m of the vortex center. The
 170 locations of these maxima and minima are used to determine an average radius (r) of maximum
 171 winds (V).

172
 173

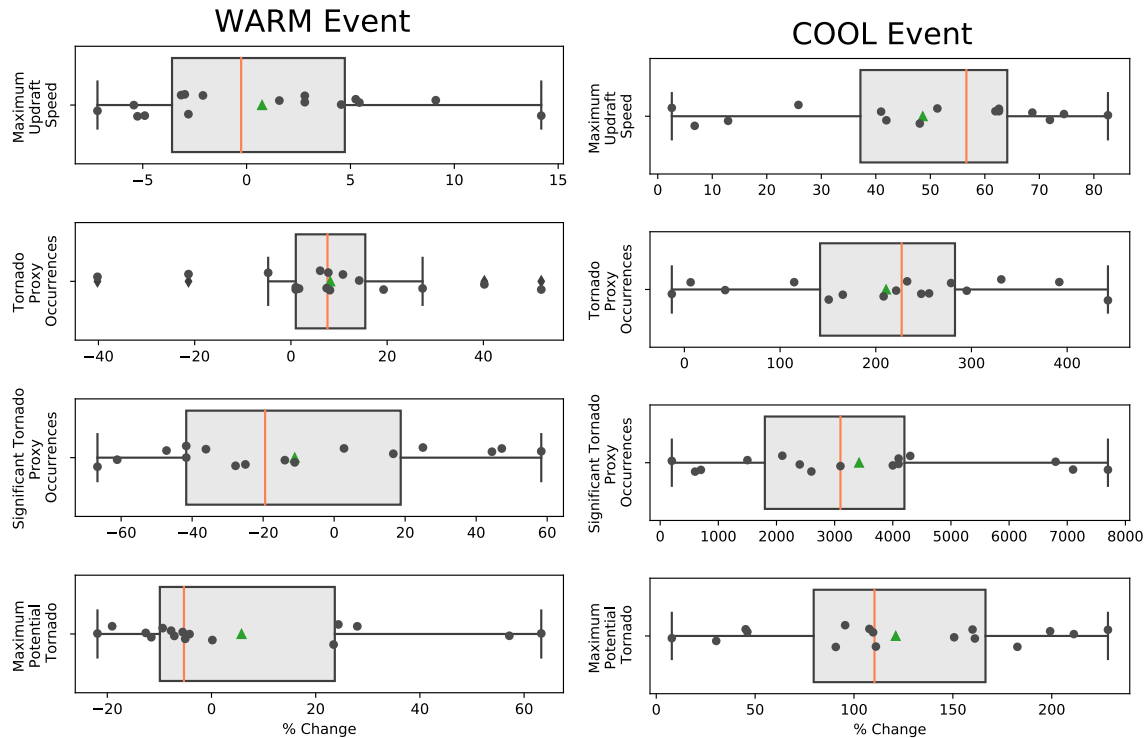


174



175
 176
 177
 178
 179
 180
 181
 182

Figure 1. Locations of tornado proxies (magenta dots) for the regional-modeling simulations of the WARM event during the hour ending 2100 UTC (upper panels), and COOL event during the hour ending 2230 UTC (lower panels). The size of the dots correspond nonlinearly to the VV associated with the proxy. The subpanels indicate the individual experiments composing the ensemble.



183

184 **Figure 2.** Box-and-whisker plots of tornadic-storm intensity metrics, as evaluated from the
 185 regional modeling simulations of the WARM event (left) and COOL event (right). Values of
 186 these metrics are given as percentage changes in the PGW simulations relative to the CTRL
 187 simulation. The median is the orange line, mean is the green triangle, and individual data points
 188 are the black circles.

189

190 3 Results

191 3.1 Regional-modeling perspective

192 An ensemble of 16 simulations is used to assess the PGW response of each event. The
 193 ensemble members represent a range of possible future realizations of the event. Herein, if 75%
 194 of the ensemble members exhibit the same sign in the percentage change (PGW relative to
 195 CTRL) in a given metric, we consider the PGW response for that metric to be *consistent*. If we
 196 equate the signal in the metric to the mean value across the ensemble, and the noise to the

197 standard deviation, the response in this metric is considered to be *robust (highly robust)* if the
198 PGW signal-to-noise ratio in a given metric exceeds one (two) (e.g., Diffenbaugh et al., 2013).

199 We begin with two metrics that provide information on overall storm intensity. The first
200 is the cumulative gridpoint exceedance of 55 dBZ simulated radar reflectivity (Figs. S2 and S3).
201 This metric quantifies the total area of intense convective storms over a given simulation. A
202 consistent, robust response is shown in this metric, as represented by a mean percentage increase
203 of +110% (PGW exceedances relative to those in the CTRL) (Fig. S3). Thus, the PGW-modified
204 conditions resulted in relatively more extensive and intense convective storms in association with
205 the WARM event.

206 Cumulative gridpoint exceedances of simulated updraft speed confirm this increase in the
207 extent of intense convective storms under PGW (Figs. S3 and S4); a consistent, robust response
208 is represented by a mean percentage increase of +40%. The *peak* updraft speeds are
209 comparatively stronger in only half of the PGW simulations, with a mean percentage increase of
210 +1% (Fig. 2). These results indicate that intense convective updrafts in a late 21st century
211 realization of the WARM event would be more numerous or larger, but not always stronger.

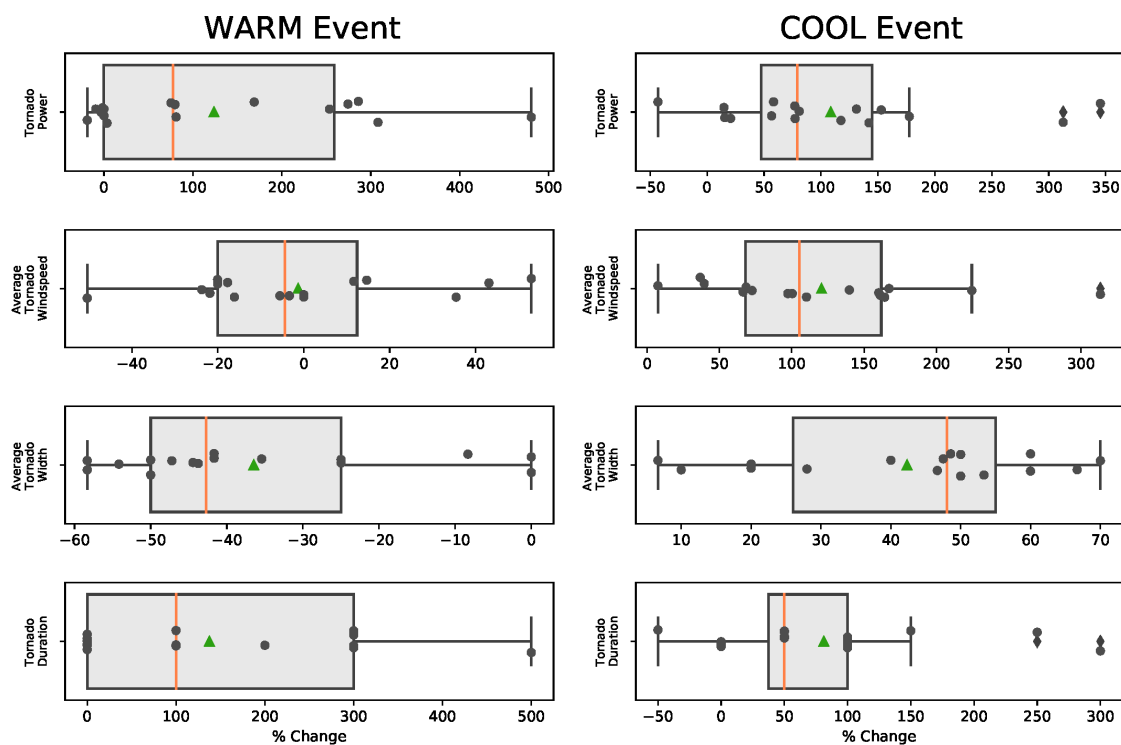
212 The PGW response in occurrences of our tornado proxy is consistent albeit not robust,
213 with a mean percentage increase of 8% (Fig. 2). The mean response occurrences of our
214 significant tornado proxy is neither consistent nor robust, with a mean percentage decrease of -
215 11% (Fig. 2). Finally, the peak VV per PGW simulation, which provides some information about
216 the *potential* tornado intensity, is also neither consistent nor robust, with a mean percentage
217 increase of 5% (and median percentage decrease of -5%) (Fig. 2). Thus, the regional modeling
218 suggests relatively more but not necessarily stronger tornadic circulations in a late 21st century
219 realization the WARM event, albeit with large uncertainty (see also Fig. 1).

220 Like the WARM event, the COOL event under PGW also tends to be characterized by
221 more intense convective storms. Specifically, cumulative gridpoint exceedances of simulated
222 reflectivity of 55 dBZ are greater in all but one of the PGW simulations, thus contributing to an
223 average percentage increase of +125%, and a consistent and robust response in this metric (Figs.
224 S2 and S3). The other metric for overall storm intensity, cumulative gridpoint exceedances of
225 updraft speed of 25 m s^{-1} , is consistent but not robust; notably, the average percentage increase in
226 such strong updraft occurrence in the COOL event is +712%, as compared to the +40% increase
227 associated with the WARM event (see Figs. S2 and S3). *All* PGW simulations had peak updraft
228 speeds exceeding the 31 m s^{-1} peak of the CTRL (Fig. 2), thus implying a consistent and robust
229 response. Moreover, half of the PGW simulations had peak updrafts exceeding 50 m s^{-1} , which
230 historically are speeds more readily supportive in warm-season, Great Plains environments than
231 in cool-season, southeast U.S. environments. These results indicate that intense convective
232 updrafts in a late 21st century realization of the COOL event would be more numerous *and*
233 stronger.

234 Occurrences of the tornado proxy are substantially greater under PGW in many of the
235 simulations, leading to a mean percentage increase relative to CTRL of +211% (Fig. 2).
236 Occurrences of the significant tornado proxy are also substantially greater, with a mean
237 percentage increase of +3244%, in this consistent and robust response (Fig. 2). Finally, a
238 consistent and robust response is indicated in the peak VV per PGW simulation, and thus
239 potential tornado intensity, with an average percentage increase of +121% (Fig. 2).

240 Collectively, these results suggest that tornadic circulations in a late 21st century
241 realization of the COOL event would be more numerous and stronger. In agreement with our
242 hypothesis, the magnitude of the response of this archetypal cool-season event to PGW is much

243 larger than that of the archetypal warm-season event; this finding is also in agreement with
 244 Bercos-Hickey et al. (2021). There is still ambiguity, however, in precisely how the analyzed
 245 response relates to tornado intensity, given both the model grid resolution and the nature of the
 246 tornado proxy. Thus, we now use the TLV-resolving idealized PGW simulations to compute
 247 explicit measures of tornado intensity, and thus help clarify the regional-model results.
 248



249

250

251 **Figure 3.** As in Figure 2, except for tornado intensity metrics (see text).

252

253 3.2 Idealized modeling perspective

254 The idealized PGW simulations have steady, horizontally homogeneous initial and
 255 boundary conditions that were drawn from the regional-model simulations of the WARM and
 256 COOL events (Figs. S5-S6). The much finer grid spacings (64 m) allow for explicit
 257 quantifications of TLVs that form within the simulated storms. For this we use *tornado power*,

258 which accounts for the tornadic wind speed as well as the width and length of the tornado track.
 259 As adapted from Fricker et al. (2014), instantaneous tornado power can be calculated as

$$260 \quad P = \pi r^2 \rho V^3 \quad (1)$$

261 where r represents the average radius of maximum winds, ρ is the air density (assumed to be 1
 262 kg m⁻³), and V is the average maximum surface wind speed at radius r . Total tornado power here
 263 is the summation of $\log(P)$ over the lifetime of the tornado-like vortex,

$$264 \quad P_t = \sum \log(P) \quad (2)$$

265 In simulations of the WARM event, the PGW response in total power is neither consistent nor
 266 robust. However, the 16-member ensemble contributed to a mean percentage increase in P_t of
 267 +124% (Fig. 3). This percentage increase is due to a few experiments with relatively stronger
 268 vortex windspeeds; none of the experiments exhibited wider vortices (Fig. 3). Thus, as in the
 269 coarser-resolution regional modeling simulations, there are indications of intensity increases in
 270 this violent, Great Plains, warm-season tornado given an imposed climate change, but with large
 271 uncertainty.

272 For the COOL event, the PGW response in total power is both consistent and robust, with
 273 an average percentage increase of +109% (Fig. 3). The increases in P_t are driven by consistent
 274 and robust increases in tornadic-vortex strength and width (Fig. 3). The relatively longer duration
 275 of the tornadic vortices (+81%) also contribute to the larger P_t under PGW. These high-
 276 resolution simulations are in agreement with the regional modeling simulations, and clearly
 277 demonstrate an increased intensity and duration for this archetypal cool-season tornado given an
 278 imposed climate change. The collective simulations also confirm our hypothesis regarding a
 279 relatively larger response of this cool-season event.

280

281 **Table 1.** Mean values, and percentage changes relative to the CTRL experiment, of
 282 environmental parameters computed from the initial/boundary conditions of the idealized-
 283 modeling PGW experiments.
 284

| Event | CAPE | | CIN | | LCL | | SRH3 | | SRH1 | | S06 | | STP | |
|-------|--------|------|--------|------|------|-----|-----------------------------------|-----|-----------------------------------|-----|-------|-----|-----|------|
| | (J/kg) | | (J/kg) | | (m) | | (m ² /s ²) | | (m ² /s ²) | | (m/s) | | | |
| WARM | 4484 | +56 | 0 | +100 | 1774 | +23 | 86 | -58 | 34 | -53 | 24 | -14 | 0.2 | -72 |
| COOL | 1037 | +162 | -24 | -61 | 243 | +33 | 427 | -21 | 327 | -23 | 36 | -4 | 2.2 | +100 |

285 CIN is convective inhibition; LCL is lifting condensation level; SRH3 is storm-relative
 286 environmental helicity, evaluated over the 0-3 km layer; SRH1 is storm-relative environmental
 287 helicity, evaluated over the 0-1 km layer; S06 is the bulk wind shear, evaluated over the 0-6 km
 288 layer.
 289

290 We can use the ic/bc of the idealized experiments to explore the meteorological
 291 arguments on which this hypothesis is based. The mean, PGW-enhanced CAPE of 4484 J kg⁻¹
 292 and 1037 J kg⁻¹ for the WARM and COOL events, respectively, represent consistent and robust
 293 increases of +56% and +162% relative to the corresponding CTRL environments (Table 1). The
 294 mean, PGW-diminished VWS of 24 m s⁻¹ and 36 m s⁻¹ for the WARM and COOL events,
 295 respectively, represent consistent and robust decreases of -14% and -4% relative to the
 296 corresponding CTRL environments (Table 1); disproportionate decreases of storm-relative
 297 helicity, another measure of VWS, are also revealed for the WARM versus COOL events (-53%
 298 and -23%, respectively; Table 1). When these and other environmental parameters are combined
 299 through the multivariate parameter STP, the environment of the WARM event is found to be
 300 relatively *less* supportive of a significant tornado under PGW (mean percentage decrease of -
 301 72%), while the environment of the COOL event is relatively *more* supportive under PGW
 302 (mean percentage increase of +100%) (Table 1).
 303

303

304 3.3 Generality of the conclusions

305 Although the intensity changes described herein apply to the specific WARM and COOL
306 events simulated, all potential tornadic-storm events realized during the warm- and cool-season
307 months of consideration would be subject to the same range of climate-change perturbations. To
308 help quantify how these perturbations alone might contribute to environments of significant
309 tornadoes, STP is calculated at all points within the regional-model domain for the CTRL and
310 PGW simulations of both events (Fig. S7). The PGW – CTRL difference for each PGW
311 ensemble member represents the contribution of the monthly climate change perturbation for that
312 member (see section 2.1) to the STP change. Upon spatially averaging the PGW – CTRL
313 differences, we find that the ensemble mean STP perturbation is -0.30 for the month of May, and
314 +0.70 for the month of February. The implication is that ACC would contribute, *on average*, to
315 environments that are relatively *less* supportive of a significant tornado during May across the
316 central Great Plains U.S., and relatively *more* supportive of a significant tornado during February
317 across the southeast U.S. Such environmental changes have been noted in studies by Gensini &
318 Brooks (2018), Bercos-Hickey et al. (2021), and Lepore et al. (2021).

319

320 **4 Summary and Conclusions**

321 Evidence for the potential of ACC to lead to increases in future tornado intensity is
322 provided through a novel climate modeling study of two contemporary, archetypal, warm- and
323 cool-season tornado events. The tornadic-storm and associated vortex of the cool-season event
324 experiences a consistent and robust increase in intensity and size when virtually placed in a
325 globally warmed future via the PGW method. The tornadic-storm and associated vortex of the
326 warm-season event experiences increases in intensity in some of the virtual experiments, but the

327 response is neither consistent nor robust, and is overall weaker than in the cool-season event.
328 Consideration of other data lends support to such a disproportionate response based on season of
329 the year.

330 The preceding statement should not be interpreted to mean that *all* tornadoes will be
331 stronger in the future. The atmospheric heterogeneity arising from naturally variable large-scale
332 atmospheric circulations, high-frequency weather systems, convective storms and their residual
333 effects, and land-surface variations (e.g., see Trapp, 2013) will continue to create diverse
334 environmental conditions both supportive and non-supportive of thunderstorm formation.
335 Significant tornadogenesis within such thunderstorms will also continue to require a delicate
336 balance between VWS and CAPE, among other environmental parameters. Yet because cool-
337 season environments in the current climate tend to be characterized by very large VWS and
338 small CAPE, future increases in CAPE (decreases in VWS) due to ACC appear to be relatively
339 more conducive to (less impactful on) this balance and thus on cool-season tornado potential.

340 These findings have implications on the possible impacts of future tornadoes forming
341 outside of climatologically favored seasons, in the United States and elsewhere around the world.
342 Indeed, situational awareness of tornado risk tends to be reduced during seasons such as boreal
343 winter, which offers one explanation for high fatalities from tornadic events during these times
344 (e.g., Ashley, 2007). It follows that more intense future tornadoes would have the potential to
345 result in more fatalities and damage.

346

347 **Acknowledgments**

348 This research was supported by the National Science Foundation, award AGS 1923042. The
349 WRF simulations were conducted on the NCAR Cheyenne Computing Facility. The CM1

350 simulations were conducted on the Blue Waters Petascale Computing Facility. We thank Dr.
351 George Bryan for making available and otherwise supporting the CM1 model. We acknowledge
352 the World Climate Research Programme's Working Group on Coupled Modelling, which is
353 responsible for CMIP, and we thank the climate modeling groups indicated in section 2.1 for
354 producing and making available their model output.

355

356 **Open Research**

357 The following GCM data sets used in this study are available through the CMIP5 repository
358 (<https://esgf-node.llnl.gov/projects/cmip5/>), using these criteria: Models: GFDL-CM3,
359 MIROC5, NCAR-CCSM4, IPSL-CM5A-LR, and NorESM-1M; Experiments: historical and
360 RCP8.5; Ensemble: r1i1p1; Realm: atmos; and Time Frequency: 3hr or 6hr. The WRF model is
361 available at <https://www2.mmm.ucar.edu/wrf/users/>, and the CM1 model is available at
362 <https://www2.mmm.ucar.edu/people/bryan/cm1/>. Relevant simulation data are available through
363 the Illinois Data Bank at <https://databank.illinois.edu/datasets/IDB-4479773>.

364

365

366 **References**

- 367 Ashley, W. S. (2007). Spatial and Temporal Analysis of Tornado Fatalities in the United States:
368 1880–2005. *Weather and Forecasting*, 22(6), 1214–1228.
369 <https://doi.org/10.1175/2007WAF2007004.1>
- 370 Bercos-Hickey, E., Patricola, C. M., & Gallus, W. A. (2021). Anthropogenic Influences on
371 Tornadoic Storms. *Journal of Climate*, 1–57. <https://doi.org/10.1175/JCLI-D-20-0901.1>

- 372 Bryan, G. H., & Fritsch, J. M. (2002). A Benchmark Simulation for Moist Nonhydrostatic
373 Numerical Models. *Monthly Weather Review*, *130*(12), 2917–2928.
374 [https://doi.org/10.1175/1520-0493\(2002\)130<2917:ABSFMN>2.0.CO;2](https://doi.org/10.1175/1520-0493(2002)130<2917:ABSFMN>2.0.CO;2)
- 375 Del Genio, A. D., Yao, M.-S., & Jonas, J. (2007). Will moist convection be stronger in a warmer
376 climate? *Geophysical Research Letters*, *34*(16). <https://doi.org/10.1029/2007GL030525>
- 377 Diffenbaugh, N. S., Scherer, M., & Trapp, R. J. (2013). Robust increases in severe thunderstorm
378 environments in response to greenhouse forcing. *Proceedings of the National Academy of*
379 *Sciences*. <https://doi.org/10.1073/pnas.1307758110>
- 380 Frei, C., Schär, C., Lüthi, D., & Davies, H. C. (1998). Heavy precipitation processes in a warmer
381 climate. *Geophysical Research Letters*, *25*(9), 1431–1434.
382 <https://doi.org/10.1029/98GL51099>
- 383 Fricker, T., Elsner, J. B., Camp, P., & Jagger, T. H. (2014). Empirical estimates of kinetic energy
384 from some recent U.S. tornadoes. *Geophysical Research Letters*.
385 <https://doi.org/10.1002/2014GL060441>
- 386 Gensini, V. A., & Brooks, H. E. (2018). Spatial trends in United States tornado frequency. *Npj*
387 *Climate and Atmospheric Science 2018 1:1*, *1*(1), 1–5. [https://doi.org/10.1038/s41612-018-](https://doi.org/10.1038/s41612-018-0048-2)
388 [0048-2](https://doi.org/10.1038/s41612-018-0048-2)
- 389 Gensini, V. A., Ramseyer, C., & Mote, T. L. (2014). Future convective environments using
390 NARCCAP. *International Journal of Climatology*, *34*(5), 1699–1705.
391 <https://doi.org/10.1002/joc.3769>
- 392 Gray, K., & Frame, J. (2021). The impact of midlevel shear orientation on the longevity of and
393 downdraft location and tornado-like vortex formation within simulated supercells. *Monthly*
394 *Weather Review*, *149*, 3739–3759, <https://doi.org/10.1175/MWR-D-21-0085.1>

- 395 Hoogewind, K. A., Baldwin, M. E., & Trapp, R. J. (2017). The Impact of Climate Change on
396 Hazardous Convective Weather in the United States: Insight from High-Resolution
397 Dynamical Downscaling. *Journal of Climate*, *30*, 10081–10100.
398 <https://doi.org/10.1175/JCLI-D-16-0885.1>
- 399 Kimura, F., & Kitoh, A. (2007). *Downscaling by pseudo global warming method. In Final report*
400 *to the ICCAP*. Kyoto, Japan.
- 401 Lepore, C., Abernathy, R., Henderson, N., Allen, J. T., & Tippett, M. K. (2021). Future Global
402 Convective Environments in CMIP6 Models. *Earth's Future*, e2021EF002277.
403 <https://doi.org/https://doi.org/10.1029/2021EF002277>
- 404 Naylor, J., & Gilmore, M. S. (2012). Convective Initiation in an Idealized Cloud Model Using an
405 Updraft Nudging Technique. *Monthly Weather Review*, *140*(11), 3699–3705.
406 <https://doi.org/10.1175/MWR-D-12-00163.1>
- 407 NOAA. (2013). NCEI Storm Events Database. Retrieved from
408 <https://www.ncdc.noaa.gov/stormevents/>
- 409 NOAA. (2022). NOAA National Centers for Environmental Information (NCEI) U.S. Billion-
410 Dollar Weather and Climate Disasters (2022). <https://doi.org/10.25921/stkw-7w73>
- 411 Sato, T., Kimura, F., & Kitoh, A. (2007). Projection of global warming onto regional
412 precipitation over Mongolia using a regional climate model. *Journal of Hydrology*, *333*(1),
413 144–154. <https://doi.org/https://doi.org/10.1016/j.jhydrol.2006.07.023>
- 414 Schär, C., Frei, C., Lüthi, D., & Davies, H. C. (1996). Surrogate climate-change scenarios for
415 regional climate models. *Geophysical Research Letters*, *23*(6), 669–672.
416 <https://doi.org/10.1029/96GL00265>

- 417 Seeley, J. T., & Romps, D. M. (2015). The Effect of Global Warming on Severe Thunderstorms
418 in the United States. *Journal of Climate*, 28(6), 2443–2458. [https://doi.org/10.1175/JCLI-D-](https://doi.org/10.1175/JCLI-D-14-00382.1)
419 14-00382.1
- 420 Sherburn, K. D., & Parker, M. D. (2019). The development of severe vortices within simulated
421 high-shear, low-CAPE convection. *Monthly Weather Review*. [https://doi.org/10.1175/MWR-](https://doi.org/10.1175/MWR-D-18-0246.1)
422 D-18-0246.1
- 423 Skamarock, W. C., Klemp, J. B., Dudhia, J., Gill, D. O., Barker, D. M., Huang, X.-Y., et al.
424 (2008). *A description of the Advanced Research WRF version 3. NCAR Tech. Note TN-*
425 *475+STR*.
- 426 Skamarock, W. C. (2004). Evaluating Mesoscale NWP Models Using Kinetic Energy Spectra.
427 *Monthly Weather Review*, 132(12), 3019–3032. <https://doi.org/10.1175/MWR2830.1>
- 428 Strader, S. M., Ashley, W. S., Pingel, T. J., & Krmenc, A. J. (2017). Projected 21st century
429 changes in tornado exposure, risk, and disaster potential. *Climatic Change*, 141(2), 301–313.
430 <https://doi.org/10.1007/s10584-017-1905-4>
- 431 Tang, B. J., Gensini, V. A., & Homeyer, C. R. (2019). Trends in United States large hail
432 environments and observations. *Npj Climate and Atmospheric Science*,
433 <https://doi.org/10.1038/s41612-019-0103-7>
- 434 Taylor, K. E., Stouffer, R. J., & Meehl, G. A. (2012). An Overview of CMIP5 and the
435 Experiment Design. *Bulletin of the American Meteorological Society*, 93(4), 485–498.
436 <https://doi.org/10.1175/BAMS-D-11-00094.1>
- 437 Taszarek, M., Allen, J. T., Marchio, M., & Brooks, H. E. (2021). Global climatology and trends
438 in convective environments from ERA5 and rawinsonde data. *Npj Climate and Atmospheric*
439 *Science*, <https://doi.org/10.1038/s41612-021-00190-x>

- 440 Thompson, R. L., Smith, B. T., Grams, J. S., Dean, A. R., & Broyles, C. (2012). Convective
441 Modes for Significant Severe Thunderstorms in the Contiguous United States. Part II:
442 Supercell and QLCS Tornado Environments. *Weather and Forecasting*, 27(5), 1136–1154.
443 <https://doi.org/10.1175/WAF-D-11-00116.1>
- 444 Toth, M., Trapp, R. J., Wurman, J., & Kosiba, K. A. (2012). Comparison of Mobile-Radar
445 Measurements of Tornado Intensity with Corresponding WSR-88D Measurements. *Weather
446 and Forecasting*, 28(2), 418–426. <https://doi.org/10.1175/WAF-D-12-00019.1>
- 447 Trapp, R. J. (2013). *Mesoscale-Convective Processes in the Atmosphere*. Cambridge University
448 Press.
- 449 Trapp, R. J., & Hoogewind, K. A. (2016). The realization of extreme tornadic storm events under
450 future anthropogenic climate change. *Journal of Climate*. <https://doi.org/10.1175/JCLI-D-15-0623.1>
451
- 452 Trapp, R.J., Woods, M. J., Lasher-Trapp, S. G., & Grover, M. A. (2021). Alternative
453 Implementations of the “Pseudo-Global-Warming” Methodology for Event-Based
454 Simulations. *Journal of Geophysical Research: Atmospheres*, 126(24).
455 <https://doi.org/10.1029/2021JD035017>
- 456 Trapp, R. J., Diffenbaugh, N. S., Brooks, H. E., Baldwin, M. E., Robinson, E. D., & Pal, J. S.
457 (2007). Changes in severe thunderstorm environment frequency during the 21st century
458 caused by anthropogenically enhanced global radiative forcing. *Proceedings of the National
459 Academy of Sciences*, 104(50), 19719–19723. <https://doi.org/10.1073/pnas.0705494104>
- 460 Trapp, R. J., Diffenbaugh, N. S., & Gluhovsky, A. (2009). Transient response of severe
461 thunderstorm forcing to elevated greenhouse gas concentrations. *Geophysical Research
462 Letters*, 36(1), L01703. <https://doi.org/10.1029/2008GL036203>

463 Woods, M. J. (2021). *Understanding extreme tornado events under future climate change*

464 *through the pseudo-global warming methodology*. University of Illinois at Urbana-

465 Champaign.

466

467